Proceedings of ICAPP '12
Chicago, USA, June 24-28, 2012
Paper 12189

Materials Corrosion in Molten LiF-NaF-KF Eutectic Salt Under Different Reduction-Oxidation Conditions

R. S. Sellers[1]*, W. J. Cheng[1, 2], M. H. Anderson[1], K. Sridharan[1], C. J. Wang[2], T. R. Allen[1]
[1]*Dept. of Engineering Physics, University of Wisconsin - Madison*
[2]*National Taiwan University of Science and Technology*
**1500 Engineering Dr. Rm. 927 Madison WI 53711*
Tel: 208-757-9203, Email: rsellers@wisc.edu

Abstract – *Molten fluoride salts such as FLiNaK (LiF-NaF-KF: 46.5-11.5-42 mol %) have been proposed for use as secondary reactor coolants, media for transfer of high temperature process heat from nuclear reactors to chemical plants, and for concentrated solar power thermal energy storage. In molten fluoride salts, passive oxide films are chemically unstable, and corrosion is driven largely by the thermodynamically driven dissolution of alloying elements into the molten salt environment.*

Two alloys, Hastelloy® N and 316L stainless steel were exposed to molten FLiNaK salt in a 316L stainless steel crucible under argon cover gas for 1000 hours at 850 °C. Graphite was present in some of the crucibles with the goal of studying corrosion behavior of relevant reactor material combinations. In addition, a technique to reduce alloy corrosion through modification of the reduction-oxidation state was tested by the inclusion of zirconium to the system.

Corrosion of 316L stainless steel was noted to occur primarily through surface depletion of chromium, an effect that was enhanced by the presence of graphite. Hastelloy® N experienced weight gain through electrochemical plating of corrosion products derived from the 316L stainless steel crucible. In the presence of zirconium, both alloys gained weight through plating of zirconium and as a result formed intermetallic layers.

I. INTRODUCTION

Generation IV nuclear initiatives have selected molten fluoride salts as a potential primary and secondary reactor coolant for transfer of high temperature process heat for hydrogen and other chemical production plants.[1] The eutectic fluoride salt mixture 46.5%LiF-11.5%NaF-42%KF (mol%), commonly referred to as FLiNaK, is emerging as a leading candidate for use as a secondary heat transfer fluid due to its advantageous thermo physical properties characterized by high thermal conductivity, high specific heat, low viscosity and high boiling point (Table I). However, at high temperatures required for a chemical processing plant, materials corrosion presents an engineering challenge due to the reduction-oxidation (redox) reaction of fluorine ions with surface protective oxide scales. Thus, the passivating properties typically exhibited by heat-resistant alloys are rendered ineffective.

Corrosion characteristics of a variety of materials in contact with molten FLiNaK salt have been studied.[2, 3, 4, 5, 6] Three major corrosion mechanisms of materials in static molten fluoride salts have been proposed. They are intrinsic corrosion, corrosion by oxidizing contaminants and galvanic corrosion.[7] Intrinsic corrosion is driven by the formation free energy of transition metal fluoride. The more negative formation free energy indicates the transition metal fluoride is more stable in fluoride salts. In other words, this transition metal has an inferior corrosion resistance to molten fluoride salt. Based on this, the corrosion resistance of the common metallic alloying elements to molten fluoride salt from low to high are ranked as the following: Al, Zr, Ti, Mn, Cr, Nb, Fe, Co, Ni, Mo and W.[2] Oxidizing contaminants in molten fluoride salts can dramatically increase the corrosion of materials. H_2O is the most common contaminant in FLiNaK due to the hygroscopic nature of one of its constituents, KF. H_2O induced corrosion includes the following reactions; HF

TABLE I
Comparison of thermo-physical properties of molten FLiNaK salt and water.

Fluid	Tm (ºC)	ρ (g/cm^3)	ρ*Cp (J/cm^3 ºC)	μ (PaS) * 10^3	k (W/m-K)	Boiling Point (ºC)
FLiNaK @ 700 ºC	454	2.02	3.81	2.9	0.92	1570 @ 1 atm.
H_2O @ 20 ºC	0	1	1.84	1	0.6	100 @ 1 atm.

TABLE II
Nominal chemical composition for 316L and Hastelloy N, wt%.
* Maximum [a] As balance

Element	C	Fe	Ni	Mn	Si	Cr	Mo
316L	0.02	[a]	10.27	1.64	0.52	17.23	2.22
Hastelloy-N	0.08*	4.12	[a]	0.66	0.76	7.30	16.19

generation (Eq. 1-2) and corrosion of metal by HF (Eq. 3).[3, 5]

$$H_2O + 2F^- \rightarrow O^{2-} + 2HF \quad (1)$$

$$H_2O + F^- \rightarrow OH^- + HF \quad (2)$$

$$M^0 + xHF \rightarrow x/2H_2 + MF_x \quad (3)$$

Where M = Ni, Fe, Cr etc.

Galvanic corrosion forms when metals with differing electromotive potentials (EMP) are conducted and exposed in molten fluoride salts. In a galvanic couple, metal with more negative EMP tends to act anodically while metal with more positive EMP tends to act cathodically. Thus, material corrosion in molten fluoride salts is accelerated due to the oxidation reaction happening at the anodic metal.[3, 5]

Two alloys, 316L stainless steel and Hastelloy® alloy N, are exposed to molten FLiNaK salt in this study. 316L stainless steel is a common low carbon Fe-Ni-Cr based alloy with wide spread industry use. 316L has the advantage of ASME code III high temperature certification and exhibits adequate long term creep rupture strength at the elevated temperatures.[8] Hastelloy® (a registered trademark of Haynes International) alloy N, referred to in this paper as Hastelloy-N, is a Ni-Mo-Cr based superalloy developed by Oak Ridge National Laboratory during the Aircraft Reactor Experiment and used as a structural alloy during the Molten Salt Reactor Experiment (MSRE) as a fluoride salt corrosion resistant material.[9, 14]

Studies dealing with molten salt chemistry have proved that control of oxidation-reduction potential is an effective method to restrain the corrosion of material in the molten salt.[10, 11, 12, 13] This technique uses sacrificial material, reductant, to maintain a reducing environment in the molten salt. In the study of Oak Ridge National Laboratory concerning redox control of the molten fluoride salts,[10] Zr has been recognized as a strong reductant, in which 4700 ppm of Cr was reduced from molten 66LiF-34BeF (mol%) salt by ~6400 ppm Zr addition. Unfortunately, the research focusing on the corrosion prevention of structural materials in the molten fluoride salts by use of reductant addition as redox control is not thoroughly investigated.

Previous static corrosion tests in molten FLiNaK salt have focused primarily on exposing a wide range of alloys to the same molten salt environment.[2, 3] The focus of this study is to expose two candidate alloys, 316L and Hastelloy-N, to molten FLiNaK salt at 850 °C for 1000 hours in 316L crucible. This is done to understand the complex material interactions between multiple materials in a practical nuclear reactor environment. In addition, Zr is added to several of the crucibles to study corrosion behavior of Hastelloy-N and 316L in a redox environment. Of the nine total crucibles, four contain metallic Zr and the remaining five do not. Olson and Ozenyara have shown the presence of graphite can aid in the corrosion of some alloys through a nonelectric transfer effect.[2, 3, 15] As some Generation IV reactor designs contain large quantities of graphite,[16] effort was also made to observe the graphite-alloy interaction in the molten FLiNaK salt environment.

II. EXPERIMENTAL

The FLiNaK used for this static test was produced in UW-Madison facilities. Source components were procured from Alfa-Aesar and Noah Technology. Fig. 1 shows the test system for the nine crucibles. All crucible components are made of 316L. 316L coupons were laser cut to size from 18 gauge sheet. Hastelloy-N coupons were taken from existing stock. The chemical compositions of the alloys are shown in Table II.

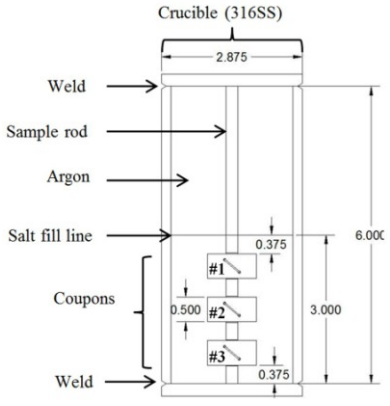

Fig. 1. Schematic view of the static corrosion test crucible. All crucible materials are made of 316L. All measurements in inches. The coupons are attached to the sample rod by 316L wire.

TABLE III
Test matrix used in this study. Crucibles 6 to 9 are labeled for clarity. 6, N, Zr and Gr used to label the crucibles 6 to 9 represent 316L, Hastelloy-N, Zr and graphite, respectively.

	Crucible 1	Crucible 2	Crucible 3	Crucible 4	Crucible 5	Crucible 6	Crucible 7	Crucible 8	Crucible 9
Label	N/A	N/A	N/A	N/A	N/A	6-Zr	6-Zr-Gr	N-Zr	N-Zr-Gr
Crucible Material	316L	316L	316L	316L	316L	316L	316L	316L	316L
Coupon 1	Hastelloy N	316L	Hastelloy N	316L	316L	316L	Hastelloy N	316L	Hastelloy N
Coupon 2	Hastelloy N	316L	Graphite	Graphite	Graphite	Graphite	Graphite	316L	Hastelloy N
Coupon 3	Hastelloy N	316L	Hastelloy N	316L	Hastelloy N	316L	Hastelloy N	316L	Hastelloy N
Redox control	N/A	N/A	N/A	N/A	N/A	Zirconium	Zirconium	Zirconium	Zirconium

The sample combination in each crucible is shown in Table III. Five of nine crucibles contained two metallic coupons and one graphite coupon located in the middle slot of the coupon stand. The purified graphite was procured from POCO, grade AFX-5Q with average particle size of 5 μm and average pore size of 0.8 μm.[17] The graphite was milled to have approximately twice the surface area of a single metallic coupon. Once all coupons and graphite pieces were tied to the sample rods in the correct order via cleaned 316L wire, they were placed in the glove box to join the salt and other crucible materials. The final steps included the addition of 513 +/- 2.5 grams of pulverized salt to each crucible followed by a finishing weld to close the crucible. Four of the nine crucibles had 10 g of pure Zr rod added to the test system. The Zr piece was positioned to rest on the bottom of the crucible. All finishing steps were performed in an argon atmosphere glove box.

During the corrosion process, samples were held at 850 °C for 1000 hours in inert nitrogen atmosphere. The corrosion levels of the samples were evaluated using weight change measurement. Characterization of the top-view and cross-sectional morphologies of the samples was carried out by scanning electron microscopy (SEM) with energy dispersive spectrometry (EDS), X-ray diffraction (XRD) and electron backscatter diffraction (EBSD).

III. RESULTS AND DISCUSSION

The results of this study are divided into two sections. The first will describe corrosion results of 316L and Hastelloy-N samples which were not in contact with Zr. The second will detail corrosion behavior of 316L and Hastelloy-N which contained Zr in the test system.

III.A. Crucibles Without Zirconium

III.A.1. Weight Change

The results of weight change of 316L and Hastelloy-N samples after FLiNaK exposure at 850 °C for 1000 hours are shown in Fig 2. Of the samples not in contact with Zr, all 316L samples lost weight during the static corrosion test while all of the Hastelloy-N samples gained weight. The presence of graphite corresponds with an increase in weight loss for 316L, while the presence of graphite appears to have no significant effect on the weight change of Hastelloy-N.

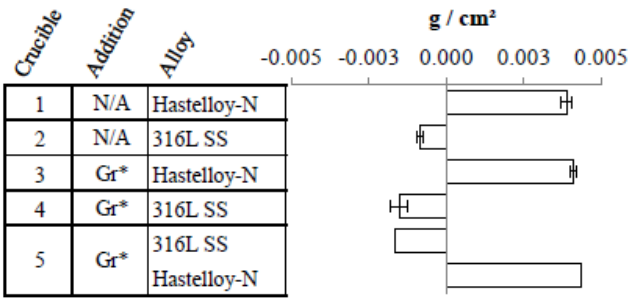

Fig. 2. Weight change of crucible 1 to 5 scenarios after corrosion testing performed in a 316L crucible filled with FLiNaK at 850 °C for 1000 hours. *Gr represents graphite.

III.A.2. 316L Stainless Steel

Fig. 3 contains cross-sectional SEM micrographs with the corresponding EDS linescan analysis of 316L samples. EDS elemental linescans from the inner 316L substrate to its surface show a relative Fe increase and Cr decrease, while Ni and Mo show no change. Also, XRD analysis reveals the surface of 316L after corrosion is γ-austenite, which is the same as 316L. These results imply that 316L experienced typical Cr dissolution behavior. Corrosion of 316L is more severe when graphite is present in the system, evident through greater measured surface Cr depletion. Approximate depth of Cr depletion for 316L and 316L with graphite is 40 μm and 50 μm, respectively.

Fig. 4 shows the change in visual characteristics of graphite samples tested with 316L. The graphite sample was covered with a silver coating. XRD identified the coating on graphite to match with Cr_7C_3. A cross-sectional SEM micrograph of the graphite samples (Fig. 5a) shows surface Cr_7C_3 formation approximately 10 μm thick. Additionally, some bright particles could be found in the Cr_7C_3. EDS revealed these bright particles to be rich in Mo and Cr, as well as a few atomic % Fe (Mo:Cr:Fe at.% ratio is 7:3:1). Phase identification of the bright particles was carried out by EBSD due to the inability of EDS to provide accurate carbon measurement. EBSD phase distribution

map of the Cr_7C_3 coating containing bright particles revealed that the bright particles are Mo_2C carbide as shown in Fig. 5b. Previous molten FLiNaK static corrosion tests performed in graphite crucibles also observed the formation of Cr_7C_3 on graphite.[3] The Cr_7C_3 and Mo_2C plating process occurs through the nonelectric transfer of Cr, Fe and Mo from 316L to electropositive graphite as described by Ozeryanaya.[15]

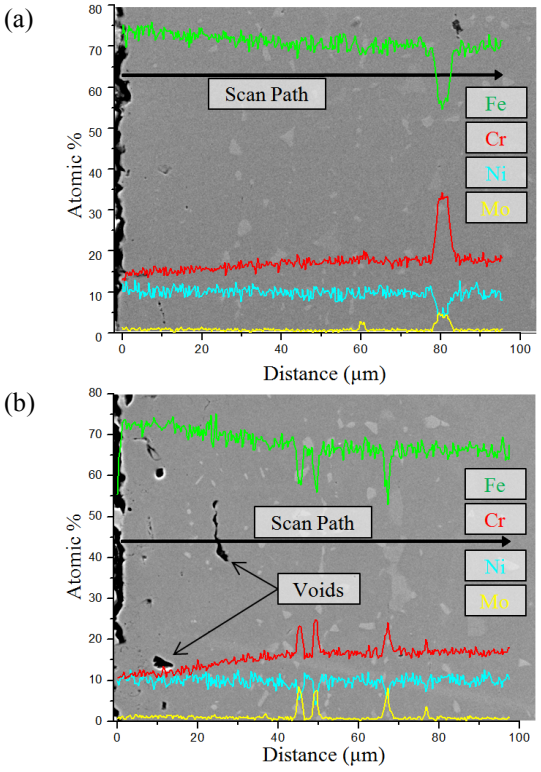

Fig. 3. Cross-sectional SEM micrographs and corresponding EDS linescan analysis of 316L samples tested (a) without graphite and (b) with graphite in FLiNaK at 850 °C for 1000 hours.

Fig. 4. (a) Typical graphite coupon appearance prior to exposure to FLiNaK at 850C for 1000 hours. (b) Graphite coupon after cleaning showing the presence of the chrome carbide coating. Sample is shorter because a cross section of the sample had been taken prior to photographing.

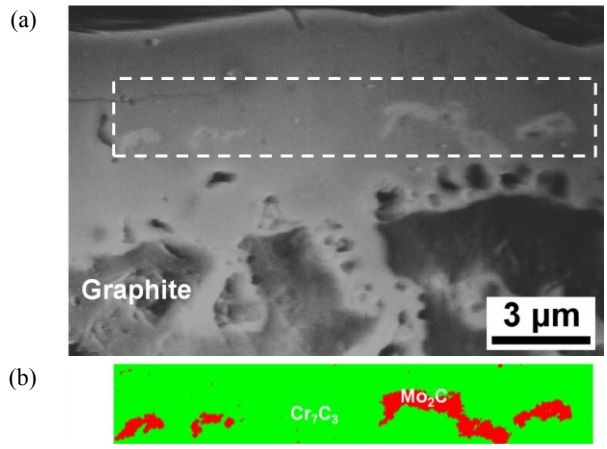

Fig. 5. (a) Cross-sectional SEM micrograph of graphite coupon tested with 316L in FLiNaK at 850 °C for 1000 hours. (b) EBSD phase distribution map of the white dotted rectangular area on SEM micrograph. Green and red phases represent Cr_7C_3 and Mo_2C, respectively. Coating on graphite sample was composed of major Cr_7C_3 and minor Mo_2C particles.

III.A.3. Hastelloy-N Superalloy

Contrary to the corrosion behavior of the 316L coupons, all Hastelloy-N samples gained weight while exposed to FLiNaK in the 316L crucible at 850 °C for 1000 hours. Fig. 6a shows the cross-sectional SEM micrographs and corresponding EDS linescan analysis of Hastelloy-N samples not in contact with graphite. From the inner substrate to the sample surface, Fe and Cr linescan profiles increased while Ni and Mo linescan profiles decreased, suggesting Ni/Mo dissolution. Although the XRD analysis shows the crystal structure of the sample surface is γ-austenite, which is the same as Hastelloy-N, the weight gain of Hastelloy-N and the formation of the Fe and Cr rich outer layer give strong evidence of a Fe/Cr deposition process instead of Ni/Mo dissolution. A similar result has been described by Kondo et. al..[5, 6] Due to the large Ni content of Hastelloy-N, it is believed the coupons acted as a cathode whereby corrosion products (Fe and Cr) dissolved from the 316L crucible plated to the surface of Hastelloy-N. This deposit process is explained through the position of Ni on electromotive potential (EMP) series in molten FLiNaK salt as shown in Table IV. Ni is more electropositive than Fe and Cr thus acts as a cathode.

Once Fe and Cr deposited on the Hastelloy-N surface, it caused the inward diffusion of Fe and Cr and outward diffusion of Ni and Mo. The cross-sectional SEM micrographs and corresponding EDS linescan analysis (Figs. 6b) reveal Hastelloy-N with the presence of graphite underwent the same Fe and Cr deposit process as Hastelloy-N without presence of graphite. However, the presence of graphite influenced the composition of the deposit layer to contain more Fe and less Cr, resulting in a larger substrate Ni diffusion. The reason for this is due to

the deposit formation on the graphite surface caused by the nonelectric transfer effect between graphite and 316L crucible, The graphite deposit has the same microstructure as observed on the graphite tested with 316L samples, major Cr_7C_3 with a small amount of Mo_2C particles. Thus, graphite can be seen as a Cr sink causing a decrease in the amount of Cr available to plate to the surface of the Hastelloy-N sample, resulting in the proportional increase of Fe in the deposit on Hastelloy-N.

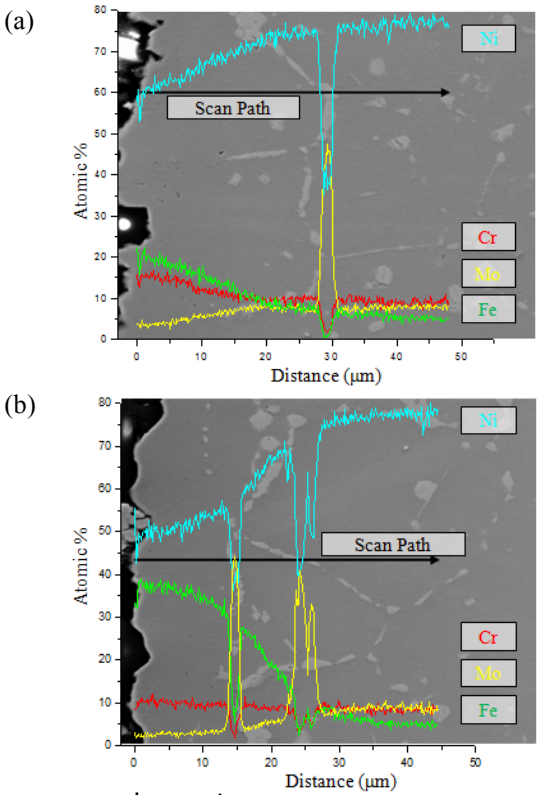

Fig. 6. Cross-sectional SEM micrographs and corresponding EDS linescan analysis of a Hastelloy-N sample tested (a) without graphite and (b) with graphite in FLiNaK at 850 °C for 1000 hours.

TABLE IV
EMP series for transition metal ions in molten FLiNaK at 750˚C in reference to the standard potential of a Ni^{2+}/Ni couple that was set to zero.[21, 22]

Half cell reaction	Standard potential (volts vs. standard Ni^{2+}/Ni electrode)
$Ni^{2+} + 2e^- = Ni$	0
$Fe^{3+} + 3e^- = Fe$	-0.21
$Fe^{2+} + 2e^- = Fe$	-0.512
$Cr^{2+} + 2e^- = Cr$	-0.69
$Cr^{3+} + 3e^- = Cr$	-1.13
$Zr^{4+} + 4e^- = Zr$	-1.25

III.B. Crucibles Containing Zirconium

III.B.1. Weight Change

Fig. 7 shows the weight change results of 316L and Hastelloy-N samples in contact with zirconium after corrosion. All of the samples gained weight after corrosion except the graphite samples in 6-Zr-Gr and N-Zr-Gr crucibles. Both graphite samples were corroded and broken into small pieces in the molten salt. The weight gain result of 316L and Hastelloy-N samples implies that some materials could deposit on the samples using molten salt as a transporting media. Additionally, the Hastelloy-N samples have a larger weight gain than the 316L samples.

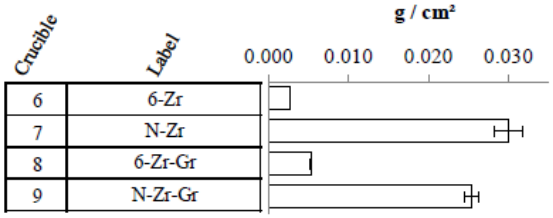

Fig. 7. Weight change of 316L and Hastelloy-N samples exposed to molten FLiNaK salt at 850 °C for 1000 hours. Graphite samples not weighted due to the breaking during exposure. See Table III for label explanation.

III.B.2. 316L Stainless Steel

The cross-sectional SEM micrographs and corresponding EDS X-ray mapping of 316L samples after corrosion are shown in Fig. 8. Both 6-Zr and 6-Zr-Gr samples possess a multiphase coating layer. The thickness of the coating on 6-Zr sample is twice that of the 6-Zr-Gr sample. The thicknesses were around 12 μm and 6 μm, respectively. Also, some crystals that embedded in the coating can only be found on the 6-Zr sample. The coatings on 6-Zr and 6-Zr-Gr possess a similar elemental distribution characteristic, that is, comprised primarily of Zr and Ni. Fig. 9 is the XRD results of the coating surfaces on 6-Zr and 6-Zr-Gr samples. It shows that Zr_3NiO and $NiZr_2$ were identified on the both samples, while ZrO_2 only existed at 6-Zr sample.

III.B.3. Hastelloy-N Superalloy

Fig. 10 displays the cross-sectional SEM micrographs and corresponding EDS X-ray mapping of Hastelloy-N samples after corrosion. Multiphase coatings can be found on N-Zr and N-Zr-Gr samples. The coatings on N-Zr and N-Zr-Gr have similar cross-sectional microstructures as well as thicknesses (~65 μm). A microstructural difference between coatings on N-Zr and N-Zr-Gr samples is that the coating on N-Zr possesses a larger number and size of

embedded crystals than the coating on N-Zr-Gr sample. The coatings on N-Zr and N-Zr-Gr possess similar characteristics of elemental distributions, comprised mainly of Zr and Ni. Also, the plan-view SEM micrographs of the coating on N-Zr and N-Zr-Gr samples reveal that the coating surface of N-Zr has a dense structure, while the coating surface of N-Zr-Gr has a porous structure. The coating surfaces on N-Zr and N-Zr-Gr samples have the similar XRD result to the 6-Zr and 6-Zr-Gr samples, in which Zr_3NiO, ZrO_2 and NiZr were identified on N-Zr samples, while Zr_3NiO and $NiZr_2$ were found on N-Zr-Gr sample.

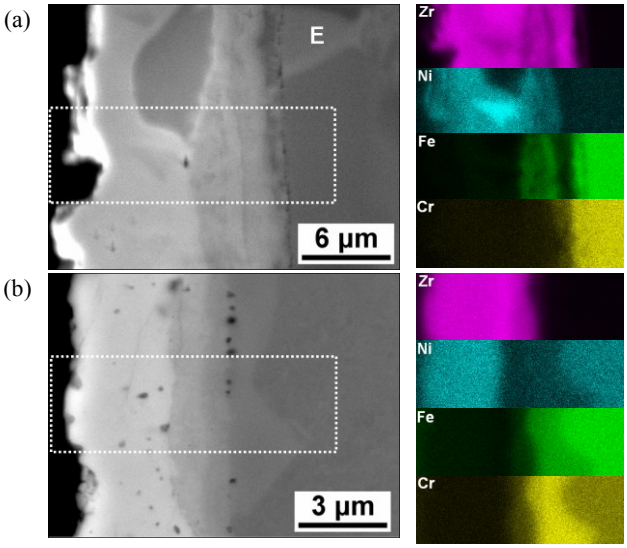

Fig. 8. SEM cross-sectional micrographs and corresponding EDS X-ray mapping of (a) 6-Zr, (b) 6-Zr-Gr samples exposed to molten FLiNaK salt at 850 °C for 1000 hours. Dotted rectangular indicates the EDS analysis area.

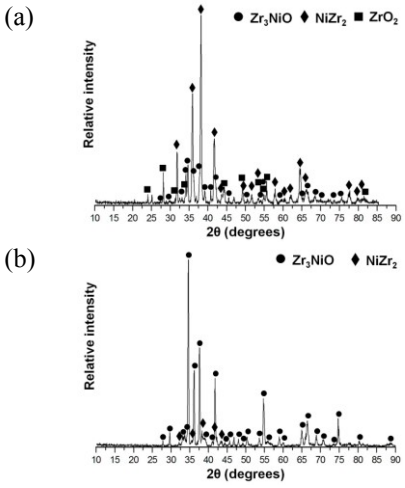

Fig. 9. XRD analysis of coating surfaces on (a) 6-Zr and (b) 6-Zr-Gr samples exposed to molten FLiNaK salt at 850 °C for 1000 hours.

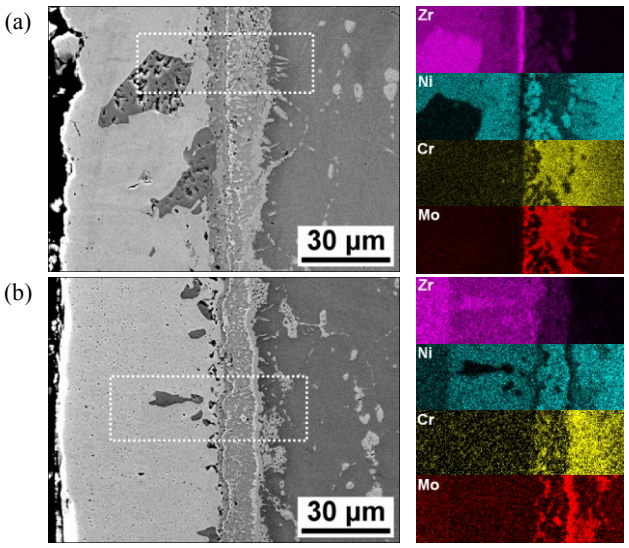

Fig. 10. SEM cross-sectional micrographs and corresponding EDS X-ray mapping of (a) N-Zr, (b) N-Zr-Gr samples exposed to molten FLiNaK salt at 850 °C for 1000 hours. Dotted rectangular indicates the EDS analysis area.

In this study, Zr addition changed the behavior of 316L and Hastelloy-N in the molten salt from corrosion of the alloys to coating formation on the alloys. The coatings are composed of major Ni-Zr binary intermetallic phases. The Ni in the coating comes from the Ni outward diffusion from the 316L and Hastelloy-N substrates, while the Zr in the coating comes from the Zr ingot transporting through the molten salt to deposit on the alloys. Thus, the formation of the coatings is due to the Zr deposition followed by the interdiffusion between the Zr deposition and substrates. The results show that the microstructure and phase constitution of the coatings are not only dominated by the Zr addition but also influenced by the graphite sample and the type of substrate. Therefore, the effects of Zr, graphite and substrate are addressed separately in the following.

III.B.4. Zirconium Addition Effect

The weight gain and microstructural results of the 316L and Hastelloy-N samples indicate the formation of the Zr deposition. The electromotive potentials of alloy element versus Ni reference electrode in FLiNaK at 750°C are -1.25 V for Zr^{4+}/Zr, -0.69 V for Cr^{2+}/Cr, -0.21 V for Fe^{2+}/Fe and 0 V for Ni^{2+}/Ni (Table IV). Zr ingot and 316L/Hastelloy-N samples formed the galvanic couples, in which Zr acted as the anode, while iron-based and nickel-based samples acted as cathode. Therefore, an anodic Zr ingot would be oxidized to form Zr ion in the molten salt, and then the Zr ion was reduced on the cathodic samples. On the other hand, ZrO_2 can be found embedded in the coating with a crystalline morphology. Research has reported that ZrO_2 can be deposited on cathodic sample by

electroplating. The ZrO_2 deposition process including oxidation of Zr (Eq. 4), hydrolysis of a partial Zr ion (Eq. 5) and dehydration of the hydroxide (Eq. 6) are as the following.[9, 18]

$$Zr \rightarrow Zr^{4+} + 4e^- \quad (4)$$
$$Zr^{4+} + 4OH^- \rightarrow Zr(OH)_4 \quad (5)$$
$$Zr(OH)_4 \rightarrow ZrO_2 + 2H_2O \quad (6)$$

The source of OH^- is coming from the H_2O contamination in the salt. It has been report that KF is a hygroscopic material, which in the case of studies performed by Kondo, caused FLiNaK to absorb 16 wt% of H_2O during the process of mixing and melting in air.[5] Zr_3NiO also can be found on all of the coatings surfaces on 316L and Hastelloy-N, being unaffected by the outer phase of the coatings is NiZr, $NiZr_2$ or $(Ni,Fe)Zr_2$ and graphite presented in the molten salt. The existence of Zr_3NiO on the coating surfaces not only indicates that the oxidation of the coating by H_2O contamination in the salt, but also implies that Zr might be able to stabilize the oxide in the molten fluoride salts.

III.B.4. Graphite Effect

According to Ozeryanaya's research of corrosion of Zr in molten chloride salt in glassy carbon crucible, finely dispersed ZrC particles have been observed in the salt.[15] The formation of ZrC particles is caused by the galvanic effect between Zr and the glassy carbon crucible, resulting in the transfer of Zr through molten salt toward the more electropositive glassy carbon crucible. However, the ZrC particles dispersed in the salt imply that the cathodic glassy carbon would still be dissolved in the galvanic process. The same result was observed in our study. The graphite samples in 6-Zr-Gr and N-Zr-Gr crucibles have been dissolved and broken into species in the salt even though graphite acted as cathode in the Zr/graphite galvanic couple. On the other hand, it can be found that the number and size of the ZrO_2 crystals embedded in the coatings on 316L and Hastelloy-N were much less when graphite was present in the salt. This result can be explained by the dissociation of ZrO_2. The process is as the following:

$$C + 4HF \rightarrow CF_4 + 2H_2 \quad (7)$$
$$ZrO_2 + CF_4 \rightarrow ZrF_4 + CO_2 \quad (8)$$

The graphite sample was initially corroded by HF (Eq. 7), which was generated by the reaction of H_2O and salt, to form CF_4. The ZrO_2 crystals growing on the sample would be corroded by CF_4 and then generated CO_2 gas (Eq. 8).[20] The porous surface of the coatings on 6-Zr-Gr and N-Zr-Gr samples can also indicate the formation of gaseous CO_2 released from the dissociation of ZrO_2. Another possible reason for reduced ZrO_2 formation is that the oxygen coming from H_2O contamination was consumed by the formation of CO or CO_2 due to the oxidation of graphite sample.

III.B.5. Substrate Effect

It has been observed that 316L sample has much smaller weight gain and coating thickness than the Hastelloy-N sample, indicating 316L sample has less Zr deposition than Hastelloy-N. This can be explained by the difference of electromotive potential between Zr and iron-based 316L being smaller than the potential between Zr and nickel-based Hastelloy-N.[21, 22] The larger difference of electromotive potential in a galvanic couple provides the higher deposition rate of anodic metal on cathode. The fact that the coating on 316L is composed of major Ni-Zr intermetallic phase even though 316L is an iron-based alloy, containing 12 wt.% Ni, is another result associated with the substrate which needs to be considered. The interdiffusion coefficient of Fe/Zr is four orders of magnitude smaller than that of Ni/Zr, providing sufficient reason for the preferential diffusion of Ni instead of Fe to the Zr layer.[23]

IV. CONCLUSIONS

IV.A. Crucibles Without Zirconium

Of the samples not in contact with zirconium, the 316L samples experienced weight loss accounted for by surface Cr depletion. When graphite was present in the system, 316L coupons have nearly double the weight loss in addition to larger void formations near the surface. This accelerated corrosion of 316L was caused by the nonelectric transfer of Cr, Fe and Mo from 316L to graphite surface to form Cr_7C_3 and Mo_2C carbides. Hastelloy-N coupons, on the other hand, form a Fe and Cr rich deposit layer on its surface. The formation of this deposit layer is due to an electrochemical plating process of 316L crucible corrosion products (Fe and Cr) on Hastelloy-N, followed by Fe and Cr inward and Ni and Mo outward diffusion. The nonelectric transfer between graphite and the 316L crucible influenced the plating behavior of Hastelloy-N by decreasing the amount of Cr available to plate to the surface, leading to a deposit composition with more Fe and less Cr than the Hastelloy-N system containing no graphite.

IV.B. Crucibles Containing Zirconium

Zr addition changed the behavior of 316L and Hastelloy-N in the molten salt from corrosion of the alloys to coating formation on the alloys. Galvanic effects between Zr and the alloys dominated the formation of the coatings. The coatings were formed by pure Zr deposition on the alloys, followed by the interdiffusion between the Zr

deposit and the substrates. The coating on Hastelloy-N has a larger thickness than the coating on 316L which can be explained by greater Zr deposition on Hastelloy-N due to the larger electromotive potential difference between Ni/Zr compared to Fe/Zr. Zr_3NiO and ZrO_2 were observed on the coating surfaces and in the coatings, respectively. The formation of Zr_3NiO and ZrO_2 oxides implies the existence of H_2O contamination in the molten salt. Graphite decreased the number and size of the ZrO_2 particles in the coatings but had no significant effect on the formation of the coatings. The fact that the interdiffusion coefficient for Ni/Zr is larger than that of Fe/Cr caused the coatings to comprise mainly of Ni-Zr intermetallic phase even though 316L is an iron-based alloy. Thus, the corrosion resistance of 316L and Hastelloy-N to molten FLiNaK salt can be enhanced by the formation of Ni-Zr coatings because the coatings can act as a barrier layer for Fe and Cr outward diffusion.

ACKNOWLEDGMENTS

The authors are very grateful to the Department of Energy of the United States of America for funding support under Grant No. **DOE-FC07-05ID14675 and DOE-FC07-07ID14826**. This research utilized NSF-supported shared facilities at the University of Wisconsin. This research is being performed using funding received from the DOE Office of Nuclear Energy's Nuclear Energy University Programs.

REFERENCES

1. D. E. HOLCOMB and S. M. Cetiner, "An Overview of Liquid-Fluoride-Salt Heat Transport Systems," *ORNL-TM-2010-156*, Oak Ridge National Laboratory, Oak Ridge, Tenn., (2010).

2. L. OLSON, J. Ambrosek, K. Sridharan, M. Anderson, T. Allen, "Materials Corrosion in Molten LiF-NaF-KF Eutectic Salt," *J. Fluorine Chem.,* **130**, 67-73 (2009).

3. L. OLSON, "Materials Corrosion in Molten LiF-NaF-KF Eutectic Salt," Ph.D. Dissertation, University of Wisconsin-Madison, Madison, WI, USA (2009).

4. A. K. MISRA, J. D. Whittenberger, in: *Proceedings of the 22nd Intersociety Energy Conversion Engineering Conference cosponsored by the AIAA ANS ASME SAE IEEE ACS and AIChE* Philadelphia, PA, *AIAA-87-9226*, 10–14 (1987)

5. M. KONDO, T. Nagasaka, Q. Xu, T. Murogaa, A. Sagara, N. Noda, D. Ninomiya, M. Nagura, A. Suzuki, T. Terai, N. Fujii, "Corrosion characteristics of reduced activation ferritic steel, JLF-1 (8.92Cr–2W) in molten salts Flibe and Flinak," *Fusion Eng. Des,.* **84**, 1081-1085 (2009).

6. M. KONDO, T. Nagasaka, V. Tsisar, A. Sagara, T. Muroga, T. Watanabe, T. Oshima, Y. Yokoyama, H. Miyamoto, E. Nakamura, N. Fujii, "Corrosion of reduced activation ferritic martensitic steel JLF-1 in purified Flinak at static and flowing condition," *Fusion Eng. Des.,* **85**, 1430-1436 (2010).

7. M. S. SOHAL, M. A. Ebner, P. Sabharwall, P. Sharpe, "Engineering Database of Liquid Salt Thermophysical and Thermochemical Properties," *INL-EXT-10-18297* (2010).

8. AMERICAN SOCIETY OF MECHANICAL ENGINEERS, *ASME Boiler and Pressure Vessel Code,* Section III Rules for Construction of Nuclear Facility Components - Division 1: Subsection NH - Class 1 Components in Elevated Temperature Service, American Society of Mechanical Engineers, United States of America (2007).

9. J. H. DEVAN, "Effect of Alloying Additions on Corrosion Behavior of Nickel-Molybdenum Alloys in Fused Fluoride Mixtures," *ORNL-TM-2021*, Oak Ridge National Laboratory, Oak Ridge, Tenn. (1969)

10. J. H. SHAFFER, "Preparation and handing of salt mixtures for the molten salt reactor experiment," *ORNL-4616* (1971).

11. J. R. KEISER, J. H. Devan, and D. L. Manning, "The Corrosion of Type 316 Stainless Steel to Li_2BeF_4," *ORNL-TM-5782* (1977).

12. G.. D. DEL CUL, D. F. Williams, L. M. Toth, Redox "Potential of Novel Electrochemical Buffers Useful for Corrosion Prevention in Molten Fluorides," *Proceedings of the Thirteenth International Symposium on Molten Salts Held during the 201st meeting of the Electrochemical Society*. p. 12-17, Philadelphia, PA, USA (2002).

13. D. OLANDER, "Redox condition in molten fluoride salts Definition and control," *J. Nucl. Mater.,* **300**, 270-272 (2002).

14. P. N. HAUBENREICH and J. R. Engel, "Experience with the Molten Salt Reactor Experiment," *Nucl. Appl. Technol.*, **8**, 118 (1970).

15. I. N. OZERYANAYA, V. Tkhai, M. V. Smirnov, E.A. Burakova, "Effect of container material on reaction of

zirconium with molten strontium chloride," Tr. Inst. Elektrokhim., Ural. Nauch. Tsentr. Akad. Nauk SSSR., **20,** 86-89 (1973).

16. U.S. DOE Nuclear Energy Research Advisory Committee, & Generation IV International Forum. "*A Technology Roadmap for Generation IV Nuclear Energy Systems.*" (2002).

17. POCO Inc, AXF-5Q, URL: http://www.poco.com/MaterialsandServices/Graphite/IndustrialGrades/AXF5Q/tabid/89/Default.aspx

18. L. GAI-OR, I. Silberman, R. Chaim, Electrolytic ZrO_2 Coatings, *J. Electrochem. Soc.,* **138**, 1939-1942 (1991).

19. F. HOU, W. Wang, H. Guo, "Effect of the dispersibility of ZrO_2 nanoparticles in Ni-ZrO_2 electroplated nanocomposite coatings on the mechanical properties of nanocomposite coatings," *Appl. Surf. Sci.,* **252**, 3812-3817 (2006).

20. D. DEVILLIERS, M. Vogler, F. Lantelme, M. Chemla, "Mass spectrometric analysis of thermal decomposition products of graphite fluorides and electrogenerated carbon-fluorine compounds," *Anal. Chim. Acta.,* **153**, 69-82 (1983).

21. A. GIRGINOV, T. Z. Tzvetkoff, M. Bojinov, "Electrodeposition of refractory metals (Ti, Zr, Nb, Ta) from molten salt electrolytes," *J. Appl. Electrochem.,* **25,** 993-1003 (1995).

22. G. MELLORS, S. Senderoff, "Electrode Reactions in the Electrolysis of Fused Salts, in G. Fitterer, (Eds)," *Applications to fundamental thermodynamics to metallurgical processes*, Gordon and Breach Science Publishers, New York, 81-103 (1967).

23. K. BHANUMURTHY, G. B. Kale, S. K. Khera, "Reaction diffusion in the zirconium-iron system," *J. Nucl. Mater.,* **185**, 208-213 (1991).